Review of Scientific Instruments

A high temperature gas flow environment for neutron total scattering studies of complex materials

Cite as: Rev. Sci. Instrum. **89**, 092906 (2018); https://doi.org/10.1063/1.5033464
Submitted: 05 April 2018 . Accepted: 14 July 2018 . Published Online: 25 September 2018

Daniel Olds, Rebecca A. Mills, Marshall T. McDonnell, Jue Liu, Joshua R. Kim, Matthew T. Dunstan, Michael W. Gaultois, S. Michelle Everett, Matthew G. Tucker, and Katharine Page

A high temperature gas flow environment for neutron total scattering studies of complex materials

Daniel Olds,[1] Rebecca A. Mills,[1] Marshall T. McDonnell,[1] Jue Liu,[1] Joshua R. Kim,[1] Matthew T. Dunstan,[2] Michael W. Gaultois,[3] S. Michelle Everett,[1] Matthew G. Tucker,[1] and Katharine Page[1]

[1]*Neutron Scattering Division, Oak Ridge National Laboratory, Oak Ridge, Tennessee 37831-6454, USA*
[2]*Department of Chemistry, University of Cambridge, Cambridge, United Kingdom*
[3]*Leverhulme Research Centre for Functional Materials Design, The Materials Innovation Factory, Department of Chemistry, University of Liverpool, 51 Oxford Street, Liverpool L7 3NY, United Kingdom*

(Received 5 April 2018; accepted 14 July 2018; published online 25 September 2018)

We present the design and capabilities of a high temperature gas flow environment for neutron diffraction and pair distribution function studies available at the Nanoscale Ordered Materials Diffractometer instrument at the Spallation Neutron Source. Design considerations for successful total scattering studies are discussed, and guidance for planning experiments, preparing samples, and correcting and reducing data is defined. The new capabilities are demonstrated with an *in situ* decomposition study of a battery electrode material under inert gas flow and an *in operando* carbonation/decarbonation experiment under reactive gas flow. This capability will aid in identifying and quantifying the atomistic configurations of chemically reactive species and their influence on underlying crystal structures. Furthermore, studies of reaction kinetics and growth pathways in a wide variety of functional materials can be performed across a range of length scales spanning the atomic to the nanoscale. *Published by AIP Publishing.* https://doi.org/10.1063/1.5033464

I. INTRODUCTION

As materials for a secure and sustainable future continue to trend toward increasing complexity, the need for insights into materials while they are in use has never been greater. We must expand the frontiers of real time analysis of functional materials to understand and control material pathways, intermediates, metastable components, defects, and interfaces and their relationships to desirable material properties. This is particularly true in large swaths of the energy sector, where our understanding of gas-solid-phase interactions remains largely conceptual. For instance, in heterogeneous catalysis, the identities, concentrations, structures, and roles of chemically reactive species remain elusive because we still lack robust approaches to observe them at relevant atomistic length or time scales. The case is similar for tracking the local and long-range interactions that define the processes of gas adsorption, storage, and separation, or the growth, coarsening, or decomposition of electrochemical components through cycling.

The pair distribution function (PDF) analysis based on neutron or x-ray total scattering techniques has emerged as an important tool in the investigation of complex material phenomena. Total scattering holds the key to determining the local material structure as well as the crystallographic average structure, often critical to understanding the underlying chemical and physical properties of functional materials. By virtue of its interactions with atomic nuclei, neutron total scattering offers particular sensitivity to the light atom surface species encountered in adsorbate, separation, and catalysis surface science; to neighboring atoms in the periodic table often encountered in transition metal containing materials; and to specific isotopes through isotope contrast experiments.[1] Additionally, the low neutron absorption cross section of materials means comparatively large volumes of samples can be penetrated relative to x-ray scattering approaches, ensuring bulk (rather than surface) measurements of structures. Several gas dosing environments are available at neutron diffraction instruments around the world,[2–6] although few are optimized for total scattering beamlines.[7] These typically involve a sample loaded into a closed cylindrical sample canister, an attached gas line, and a connected gas manifold for dosing and evacuation. Thermal decomposition and crystallization studies have also been completed at a number of neutron diffraction beamlines, including several at total scattering beamlines.[8–11] Surprisingly, few options exist for gas flow experiments at neutron diffraction beamlines, limiting *in situ* and *in operando* studies to date.

The Nanoscale Ordered Materials Diffractometer (NOMAD) BL-1b at the Spallation Neutron Source (SNS)[12] combines the advantages of moderate momentum transfer (Q) resolution and wide Q range time-of-flight (TOF) neutron scattering with world-leading neutron flux, making it particularly well suited among dedicated total scattering beamlines for studying the local structure of materials in their operating environments. A high precision ambient temperature gas flow environment for NOMAD was recently commissioned at the beamline,[13] offering experimental access to local and long-range structural responses to gas-solid interactions.[14] However, many industrial reactions and processes occur in conditions far above ambient temperatures, necessitating an environment that combines gas flow cell and high temperature furnace capabilities.

The primary challenge to date in developing such a capability has been achieving appropriate background scattering

contributions alongside the material and component design requirements for the high temperature regime of interest. Total scattering studies are absolutely dependent on stable background scattering: diffuse scattering often comprises a small portion of total scattering intensity in disordered crystalline systems.[15] Effort is made to maximize the amount of samples in the neutron beam while minimizing the presence of background components. It is essential to accurately measure the parasitic scattering arising from the sample container, air/ambient environment, and any other instrument background components. As much as possible, containers are made thin and of weakly scattering components (typical materials are thin amorphous quartz, incoherently scattering vanadium, or null scattering alloys such as titanium zirconium). Care is taken to ensure that corrections for absolute normalization, multiple scattering, and absorption can be completed for the chosen geometry, most often leading to cylindrical or annular sample cross sections. The temperature dependence of background and sample container scattering must also be considered and worked into experiment plans and data reduction routines. A final consideration is the thermo-mechanical integrity of sample cell components. Alternate choices are often required to avoid chemical reactivity of specific gas and sample components with sample containment components (for example, certain elements react or alloy with vanadium or titanium zirconium, or may react with quartz at elevated temperatures). A confluence of these factors has prevented the actualization of a high temperature gas flow environment for neutron PDF studies until now.

This paper describes the design and capabilities of the new high temperature gas flow environment for neutron diffraction and PDF studies available at the NOMAD instrument, SNS, intended for studying the reactive species of functional materials during their operation, including growth, dehydration, or decomposition regimes. Two commissioning examples demonstrate the utility of the new equipment: (1) a decomposition study of a battery electrode material under inert gas flow and (2) a carbonation/decarbonation cycling experiment using a carbon capture material. This technique will be useful in studying the connection between global symmetry and local symmetry and unraveling not just what happens but also why it happens through real-time studies of material functionality under gas flow conditions.

II. DESIGN AND CAPABILITY

The primary components of the high-temperature gas flow environment are the high precision gas flow system,[13] a modified vacuum furnace based off of an Institut Laue–Langevin (ILL) design,[16] a sample stick, and the custom high-temperature U-tube sample cell developed at the SNS. The capabilities and operating ranges of the high precision gas flow and furnace system as employed in this sample environment are summarized in Table I.

The quartz U-tube sample cell was designed to facilitate precise gas flow at high temperatures and strikes a balance between the sample cell structural integrity and low background. In order to operate at the standard high temperature range of 800 °C, it is necessary that the furnace hot zone be well separated from the quartz-to-stainless steel adapter as this junction has a maximum operating temperature of 450 °C. It was found that under the operating conditions, with the employed furnace, this required a minimum of 25.4 cm between the sample position and the quartz-to-stainless steel adapter. The NOMAD beamline has a beam width at sample position of roughly 1.5 cm. The quartz U-tube sample cell has an outer diameter (OD) at sample position of 4.95 ± 0.05 mm with a wall thickness of 0.38 ± 0.1 mm. In order to accommodate the NOMAD beam profile, the lateral distance of the quartz tube at the sample-position to return-side is 2 cm (center-to-center). A strain relief device is mounted directly above the stainless-steel junction to prevent tube breakage. A rendering of the installed setup is shown in Fig. 1 (left), with images of the sample stick (center) and U-tube (right) also shown. Above the quartz-to-stainless steel adapter, a $\frac{1}{4}$ in. Swagelok adapter is used to connect both the inlet and outlet flows to the sample centering stick. A set of valves at the top of the centering stick is used to isolate an installed sample cell from the atmosphere during installation and removal.

TABLE I. Overview of general operating capabilities of the high temperature gas flow sample environment.[17]

Temperature range (°C)	30–800
Heating ramp rate (°C)	0–10
Gas flow rate (ml/min)	0–50
Pressure at the sample (atm)	0–2
Gas switch time (ms)	425
RGA measurement time	250 ms per mass point

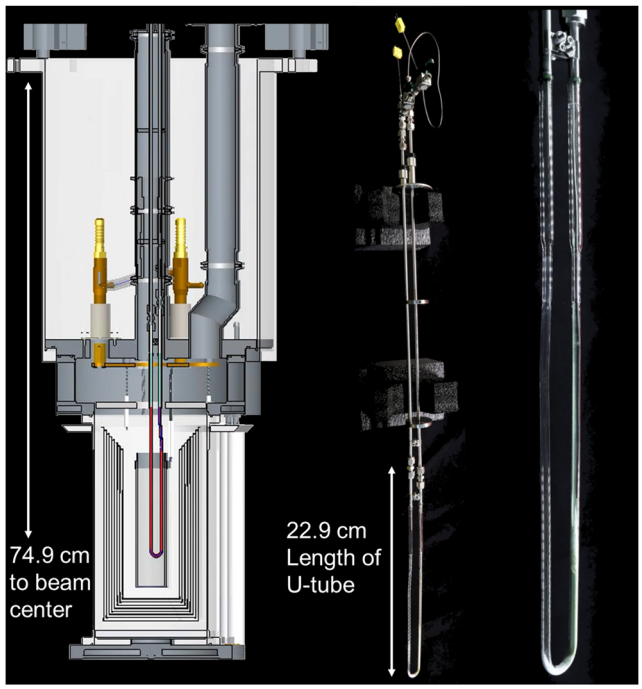

FIG. 1. (Left) Rendering of the quartz sample U-tube for high temperature gas flow cells as it is installed in the ILL-type furnace on NOMAD. (Center) Photograph of the U-tube installed on the sample centering stick and (right) zoomed-in view of the U-tube with the sample loaded.

The employed furnace is equipped with vanadium windows and has a 50 mm diameter bore hole. In this configuration, with a standard sample stick, the furnace has a maximum possible temperature of 1200 °C. However, the additional constraints brought about by the quartz-to-steel adapter limit the usable maximum temperature to 800 °C. Cooling in the furnace is passive such that the maximum cooling rate is a function of the current temperature, ranging nonlinearly from 200 °C/min at the maximum temperature of 800 °C down to 1 °C/min at 35 °C. The cooling rate can be controlled via the ramp function of the furnace while the furnace is at higher temperatures, so long as the desired cooling rate is slower than the passive cooling capacity at that temperature. Any desired cooling rates below the maxima are possible, down to the limits of precision of the furnace. Thermocouples installed inside the gas flow U-tubes, in contact with the sample, are used to control the furnace temperature via a software controlled setpoint.

Powdered samples which permit the desired flow of gas are required as the only pathway for the gas to flow is through the sample. To ensure this, offline flow testing under the planned experimental conditions is suggested. Samples which naturally do not allow sufficient flow can be pressed into a pellet, broken up, and sieved into coarse particles. Silica wool is placed above and below the sample position to maintain the correct sample height in the beam. A 3 cm or greater column of sample is suggested, with a total sample volume of 0.2 cm^3–0.6 cm^3 typically required.

III. DATA ENCODING AND REDUCTION

The measured data can be automatically reduced into common diffraction (TOPAS, GSAS, FullProf) and PDF (PDFgetN, PDFgui, RMCprofile) data formats using the Interactive Data Language (IDL)-based NOMAD instrument software.[12] However, as the measured data are encoded into a NEXUS file,[18] with associated timing, temperature, gas flow conditions, and residual gas analyzer information, advanced data reduction schemes are possible using the Mantid data reduction framework.[19]

The background measurements for this sample environment are very sensitive to subtle changes; for instance, temperature dependent changes and differences in the U-tube wall thickness will be seen clearly in measured data. As such, temperature-dependent and tube-specific data reduction methods can be employed for more precise results. Examples of data from samples loaded in the quartz U-tube, compared to the standard capillary used for most measurements on NOMAD, are found in Fig. 2. The measured scattering structure factor, S(Q), is normalized and transformed into the real-space pair-distribution function, G(r), via the equation

$$G(r) = \frac{2}{\pi}\int_0^\infty Q[S(Q) - 1]\sin(Qr)\mathrm{d}Q. \quad (1)$$

Note that G(r) is often presented in arbitrary units (a.u.) and fit using an overall scale factor due to the reduction procedures defaulting to non-absolute data corrections. Correct sample placement is critical for high-quality quantitative data analysis. Subtle differences in the thickness of the U-tubes can lead to over- or under-subtraction of the background. The characteristic pair-pair correlations in amorphous quartz at r = 1.6 Å and 2.6 Å can be used to guide the background scaling factor and verify proper reduction. If necessary, the influence of quartz peaks in the data could also be avoided through the use of a vanadium sample tube when it is compatible with sample chemistry, and oxidation or reaction with vanadium metal is not a concern.

IV. COMMISSIONING STUDY: DECOMPOSITION OF ORDERED λ-$Ni_{0.5}Mn_{1.5}O_4$

While global use and research efforts into Li-ion batteries continue to rise, significant challenges still exist surrounding safety concerns that may lead to catastrophic failure events. Concerns regarding the thermal safety of high-voltage cathode materials such as $LiMn_{1.5}Ni_{0.5}O_4$ are among some of the pressing issues facing next generation cathode compositions as O_2 release from the crystal lattice at elevated temperatures leads to significant changes in electrochemical performance and potential thermal runaway situations. The combination of both high-voltage and high thermal stability is an important material selection criterion for the design of electrochemical cells as increasing demand for high-power energy storage has periodically demonstrated catastrophic failures in commercial applications.[20,21] To better identify and understand the failure mechanisms in energy materials, such as $LiMn_{1.5}Ni_{0.5}O_4$, *in situ* studies are critical. Previous studies utilizing time-resolved x-ray diffraction[22] have identified the mechanistic pathways responsible for oxygen evolution from the crystal lattice. Local structure studies via PDF have the potential to identify the underlying mechanisms which precipitate the

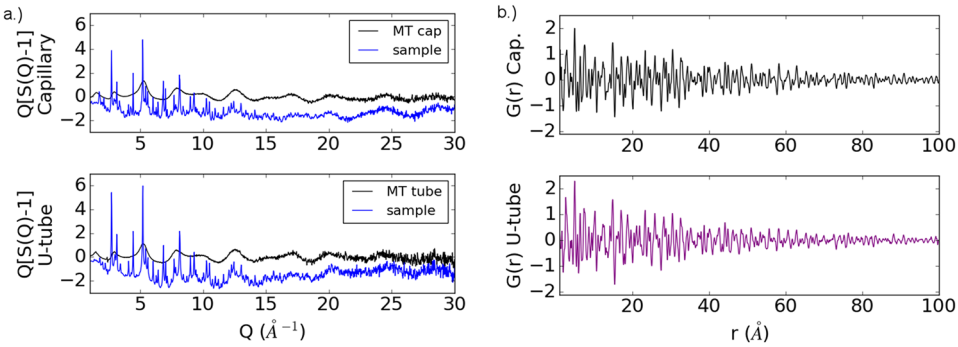

FIG. 2. (a) Comparison of the diffraction data and (b) PDF data from *ex situ* λ-$Ni_{0.5}Mn_{1.5}O_4$ samples loaded in the quartz capillary (top) vs. *in situ* samples loaded in the quartz U-tube (bottom).

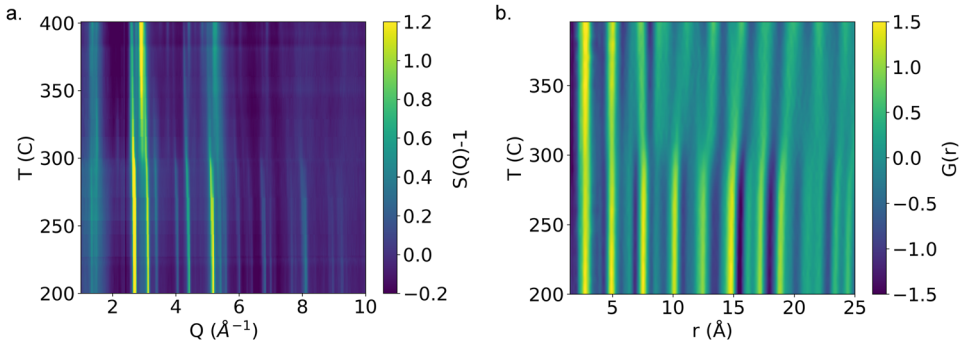

FIG. 3. (a) Diffraction and (b) PDF datasets from *in situ* decomposition measurements of λ-$Ni_{0.5}Mn_{1.5}O_4$, shown between 200 °C and 400 °C.

decomposition, as well as perhaps to suggest characteristic signatures which could indicate impending failure prior to catastrophic oxygen release. We here study the decomposition of partially ordered and delithiated $LiMn_{1.5}Ni_{0.5}O_4$ as a commissioning study of the high temperature gas flow cell environment.

$LiMn_{1.5}Ni_{0.5}O_4$ powder samples were synthesized[23] and subsequently annealed in air at 720 °C to produce the ordered ($P4_332$) spinel phase. With a sufficiently high redox potential (≈5.1 V vs. Li/Li+), NO_2BF_4 was used to chemically delithiate the as-prepared sample using a 2:1 NO_2:Li ratio in dried acetonitrile. Mixtures were left for 24 h under Ar atmosphere. Products were rinsed and filtered prior to drying under vacuum. The sample was loaded into a quartz U-tube in a He glovebox and sealed in a vacuum bag prior to transferring to the beamline. The loaded U-tube was transferred to the sample stick under constant Ar flow and purged with ultra-high purity Ar immediately prior to the measurement.

The sample was measured at room temperature in the gas flow cell isolated for 95 min and under flow at 30 SCCM Ar flow conditions for 45 min. No significant differences were seen in the measured diffraction data under an isolated inert environment compared to flow. We note that while not the disordered polymorph (verified by the presence of peaks at Q = 1.0 Å^{-1} and 1.7 Å^{-1}), these samples were only partially ordered due to the comparatively short annealing time during synthesis.

The sample was then heated at 1 °C/min up to 400 °C and soaked at temperature for 3 h. *In situ* neutron diffraction measurements were taken during this ramping and soak time, with the data initially binned into 5 min segments. The resultant diffraction and PDF from each of these 5 min sections are shown as a 2D dataset in Figs. 3(a) and 3(b). It can be seen that the reaction starts at ≈280 °C and is completed by ≈350 °C.

We first characterize the set of *in situ* data using combinatorial appraisal of transition state (CATS) analysis.[24] This allows for model-free rapid identification of similarity across a large number of data with a defined r-range. The comparisons of the local similarity (r = 0–5 Å) with longer range similarity (r = 5-40 Å) are shown in Fig. 4(a). Across these two real-space ranges, we see a much greater swell in normalized residual of data comparison in the long-range features [upper left quadrant in Fig. 4(a)] than the short-range features (lower-right quadrant). The CATS suggests that the local structure remains much more consistent across the full temperature range, despite the longer range features altering significantly at 280 °C and 350 °C. Inspection of the PDFs presented in Fig. 3(a) confirms this analysis as the local structure (r < 5 Å) is seen to change only subtly across the entire temperature range, in contrast to the significant changes seen in longer lengthscale pair-pair correlations (r > 5 Å). This suggests that the reaction pathway undertaken by the material is displacive in nature, as opposed to reconstructive or first order. Furthermore, close examination of the data, rebinned in a motif suggested by the CATS analysis, reveals the existence of an intermediary phase, shown in Fig. 4(b) (middle).

Although in-depth quantitative refinement and analysis of this *in situ* data are to be explored in future work, this preliminary analysis demonstrates the utility of performing *in situ* studies of complex materials, revealing behaviors and structures which would not be discoverable using conventional *ex situ* studies of pristine and fully decomposed samples.

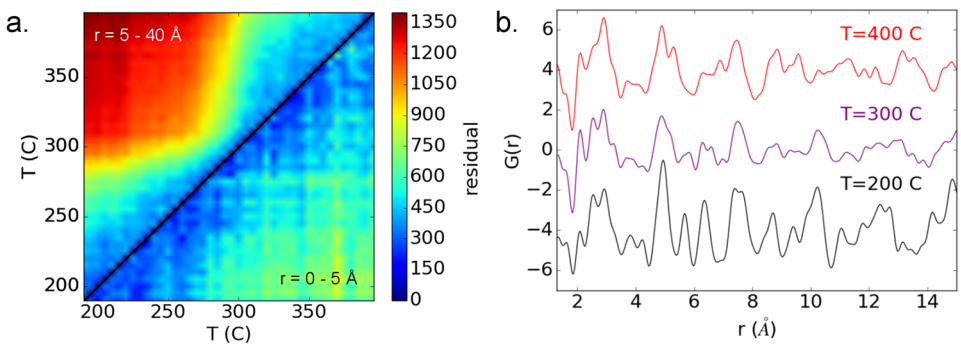

FIG. 4. (a) r-dependent CATS analysis of the PDF (plotted with a colormap based on normalized residual of the r-range) and (b) the associated data identified through the CATS analysis of the *in situ* λ-$Ni_{0.5}Mn_{1.5}O_4$ decomposition study. The decomposition process can be seen to begin around 280 °C, completing the structural transformation by 350 °C.

V. COMMISSIONING STUDY: CARBON CAPTURE VIA HIGH TEMPERATURE CARBONATION/CALCINATION CYCLING OF CALCIUM OXIDE

With growing concerns for the effects of anthropogenic greenhouse gases, particularly CO_2 and its long-term effects on our global climate, it becomes imperative to develop technologies that reduce production or release of CO_2 to the Earth's atmosphere. Carbon capture and storage (CCS) targets the latter of these two, providing a promising solution for reaching ambitious emission reduction targets set by countries around the world.[25] In power generation alone, the burning of fossil fuels leads to the release of flue gases with concentrations of CO_2 on the order of 5 vol. % (combustion of natural gas) to upwards of 12 vol. % (combustion of coal). Currently, companies are considering scrubbing the flue gas with liquid amines to selectively remove CO_2.[26] Yet, this process requires a substantial amount of energy: 15%-20% of the electrical output from the power station is required. An alternative solution is to use solid sorbents that can absorb the CO_2 at the high operating temperature of the flue gas and release the gas upon increasing temperature, providing a continuous absorber recycling loop.

One of the most promising solid sorbent materials is the CaO-$CaCO_3$ system due to its high CO_2-absorption temperature range (650-900 °C), low economic cost, and natural abundance in Ca-containing minerals such as limestone and dolomite.[27,28] In operating conditions, CO_2 is removed from the flue gas by reacting with CaO to form $CaCO_3$ (carbonation). After removing the solid from the absorbing system and with an increase in temperature, CO_2 is released and $CaCO_3$ is converted back to CaO (calcination). This allows the CaO to be recycled back into the absorber system.

While limestone is already being used in pilot plants, further research of the underlying atomistic details of this reaction is imperative to realize optimal performance of CaO-based materials for CCS. Currently, the main research focus is on improving the macroscopic properties of the system, such as the capacity and kinetics of the overall cycle, and very few studies have sought to study the mechanism of this absorption/desorption process in terms of understanding the initial formation of the carbonate layer on individual particles and the subsequent diffusion of CO_2 molecules (whether via a solid-state type ionic conduction mechanism through shell layer cracking or otherwise) to react with the unreacted core.[29,30] More detailed observation of the local nanostructures formed upon carbonation and calcination is needed to resolve this basic question of the reaction. Local structure studies via PDF prove to be a key tool in discerning the atomistic structural changes for reaction chemistry and in catalytic systems. We here study the carbonation/calcination cycling of CaO-$CaCO_3$ as another commissioning study of the high temperature gas flow cell environment.

The CaO samples were prepared from CaO nanopowders (98%, <16 nm, Sigma Aldrich). The powder was loaded into a quartz U-tube on a lab bench with silica wool below and above the sample. Initially, the sample was loaded in the furnace in the gas flow cell and taken to the elevated temperature of 900 °C to drive off any surface absorbents from exposure to the environment during loading and to ensure complete calcination to CaO.[17]

In Figs. 5(a) and 5(b), the time evolution of the carbonation/calcination cycle for both the diffraction and the PDF, respectively, is shown. Before the experiment starts at time $t = 0$ min, the sample temperature has been increased to 900 °C at 5 °C/min under a 30 SCCM N_2 gas flow. Starting at $t = 0$ min, the sample was measured for approximately 45 min to ensure it was fully calcined based on the diffraction and PDF patterns ($t = 0$ min to $t = 45$ min). The sample was then ramped down to 600 °C, and the gas flow was switched to 1 SCCM of CO_2 and 20 SCCM of N_2, corresponding to the changes observed at approximately $t = 50$ min in Fig. 5. Patterns were then collected every 5 min to give the smooth evolution of the carbonation phase transition to $CaCO_3$ observed from $t = 50$ min to $t = 125$ min. Then, the gas flow was switched back to 30 SCCM N_2 and the sample was ramped again to 900 °C to undergo calcination back to CaO ($t = 125$ min to $t = 150$ min). This corresponds to the phase change observed at approximately 125 min in Fig. 5.

In Fig. 6(a) and in Fig. 6(b), the diffraction and PDF patterns are shown, respectively, comparing representative CaO and $CaCO_3$ patterns extracted from Fig. 5. Theoretical neutron PDFs of bulk CaO and $CaCO_3$ were calculated using the GULP software package[31] to determine characteristic PDF peaks that can be attributed uniquely to either the CaO or $CaCO_3$ structure. Details of the calculations have been previously reported.[32] In Fig. 6(c), we show the simulated PDFs (dashed) compared to the experimental PDFs (solid) for CaO and $CaCO_3$, and the difference pattern of the CaO patterns subtracted from the $CaCO_3$ patterns. The characteristic 1.3 Å C–O pair distance for $CaCO_3$ can be seen to emerge in the PDF data in both Figs. 5(b) and 6(b), displaying the unique ability to track the evolution of the local atomistic CaO structure to $CaCO_3$ during carbonation using neutron total scattering. Similarly, the long-range structural changes can be observed in the differences of the diffraction patterns from Figs. 5(a)

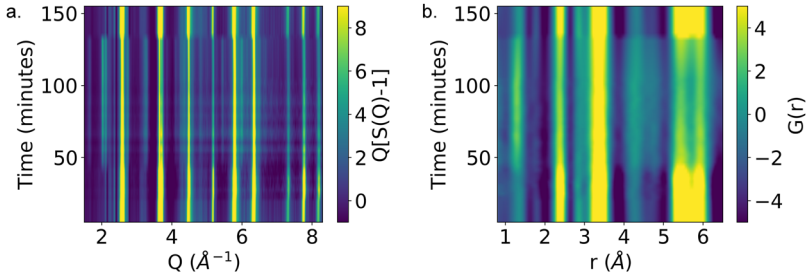

FIG. 5. (a) Full set of diffraction and (b) PDF datasets from *in situ* measurements for a carbonation/calcination cycle. This cycle begins with CaO at 900 °C ($t = 0$ min to $t = 45$ min), is ramped to 600 °C and then involves gas flow of CO_2 and N_2 to undergo carbonation to $CaCO_3$ ($t = 45$ min to $t = 125$ min), and is finally ramped back up to 900 °C to undergo calcination back to CaO ($t = 125$ min to $t = 150$ min).

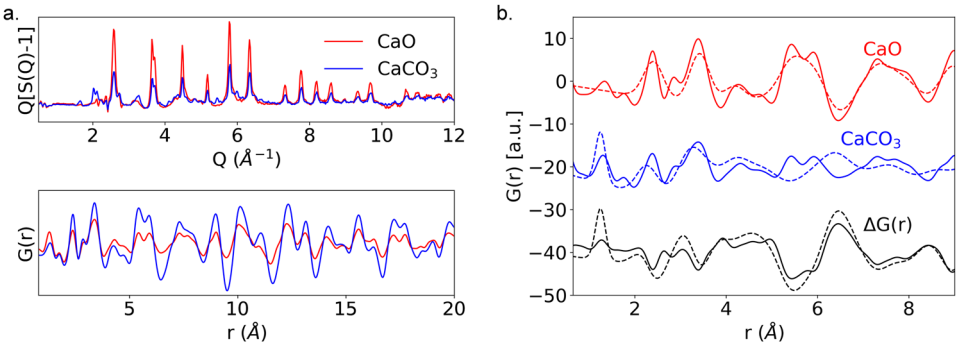

FIG. 6. Measured (a) diffraction data {plotted as $Q[S(Q) - 1]$} and PDF data. Comparison of (b) local PDF for CaO and $CaCO_3$ from experimental (solid) and simulated (dashed) patterns. The difference of the CaO subtracted from the $CaCO_3$ patterns is shown for $\Delta G(r)$.

and 6(a), for example, by the additional peak at approximately 2 $Å^{-1}$ and the reduction in the peak near 5 $Å^{-1}$ during the carbonation transition.

The high temperature gas flow cell allows for the capability to track the local atomistic structural changes coupled with the long-range, average (Bragg diffraction) structural changes *in situ* through reaction pathways, phase transitions and during catalytic reactions, as shown here with carbonation/calcination cycling for CaO-based materials. The results of this study and others like it for CCS materials can help elucidate the mechanism for the absorption/desorption process and give key insights into the atomic origins of this material functionality. Future work will follow up with in-depth quantitative refinement and mechanistic details of these *in situ* data along with studies of other new, novel solid sorbent materials measured on NOMAD with the gas flow cell furnace to further elucidate *in situ* reaction pathways for CCS materials.

VI. CONCLUSION

We have designed and commissioned a high temperature gas flow environment for neutron diffraction and PDF studies available at the NOMAD instrument, SNS. The setup combines the use of a specially designed metal-to-quartz gas flow sample tube, a high precision gas flow manifold and residual gas analyzer, an ILL vacuum furnace, and the intrinsic high flux and wide-Q range capabilities of the neutron total scattering diffractometer NOMAD. Two commissioning examples have highlighted the utility of the new equipment for following local and long-range structural responses to high temperature and/or gas flow conditions *in situ* and *in operando*. The thermal decomposition of a battery electrode material under inert gas flow was observed to have a several step and multi-lengthscale decomposition process, commencing at 200 °C and concluding at 400 °C. Temporal diffraction and PDF pattern changes in the CaO carbonation phase transition have been captured to give short and long range coupled changes and can further help elucidate the absorption/desorption mechanism for CaO to $CaCO_3$. This sample environment is currently available in the general user program at the SNS for use on the NOMAD beamline. With instrument-specific modifications, this design could be utilized on other neutron scattering beamlines at the SNS (e.g., POWGEN, CORELLI) as well as at other neutron or x-ray scattering facilities.

ACKNOWLEDGMENTS

M.W.G. thanks the Leverhulme Trust for funding via the Leverhulme Research Centre for Functional Materials Design. D.O. and K.P. were funded by the BES Early Career Award, Exploiting Small Signatures: Quantifying Nanoscale Structure and Behavior KC04062, under Contract No. DE-AC05-00OR22725. The data were measured on the Nanoscale-Ordered Materials Diffractometer (NOMAD) instrument at the Spallation Neutron Source at ORNL.

[1]P. S. Salmon, S. Xin, and H. E. Fischer, "Structure of the glassy fast-ion conductor $AgPS_3$ by neutron diffraction," Phys. Rev. B **58**, 6115 (1998).
[2]R. Haynes, S. Norberg, S. Eriksson, M. Chowdhury, C. Goodway, G. Howells, O. Kirichek, and S. Hull, "New high temperature gas flow cell developed at ISIS," J. Phys.: Conf. Ser. **251**, 012090 (2010).
[3]M. Widenmeyer, R. Niewa, T. C. Hansen, and H. Kohlmann, "*In situ* neutron diffraction as a probe on formation and decomposition of nitrides and hydrides: A case study," Z. Anorg. Allg. Chem. **639**, 285–295 (2013).
[4]L. J. McCormick, S. G. Duyker, A. W. Thornton, C. S. Hawes, M. R. Hill, V. K. Peterson, S. R. Batten, and D. R. Turner, "Ultramicroporous MOF with high concentration of vacant Cu-II sites," Chem. Mater. **26**, 4640–4646 (2014).
[5]S. Lee, H. Chevreau, N. Booth, S. G. Duyker, S. H. Ogilvie, P. Imperia, and V. K. Peterson, "Powder sample-positioning system for neutron scattering allowing gas delivery in top-loading cryofurnaces," J. Appl. Crystallogr. **49**, 705–711 (2016).
[6]R. J. Longbottom, B. Ingham, M. H. Reid, A. J. Studer, C. W. Bumby, and B. J. Monaghan, "*In situ* neutron diffraction study of the reduction of New Zealand ironsands in dilute hydrogen mixtures," Miner. Process. Extr. Metall. (published online).
[7]H.-W. Wang, V. R. Fanelli, H. M. Reiche, E. Larson, M. A. Taylor, H. Xu, J. Zhu, J. Siewenie, and K. Page, "Pressure/temperature fluid cell apparatus for the neutron powder diffractometer instrument: Probing atomic structure *in situ*," Rev. Sci. Instrum. **85**, 125116 (2014).
[8]H.-W. Wang, D. J. Wesolowski, T. E. Proffen, L. Vlcek, W. Wang, L. F. Allard, A. I. Kolesnikov, M. Feygenson, L. M. Anovitz, and R. L. Paul, "Structure and stability of SnO_2 nanocrystals and surface-bound water species," J. Am. Chem. Soc. **135**, 6885–6895 (2013).
[9]S. Lan, X. Wei, J. Zhou, Z. Lu, X. Wu, M. Feygenson, J. Neuefeind, and X.-L. Wang, "*In-situ* study of crystallization kinetics in ternary bulk metallic glass alloys with different glass forming abilities," Appl. Phys. Lett. **105**, 201906 (2014).
[10]H.-W. Wang, L. L. Daemen, M. C. Cheshire, M. K. Kidder, A. G. Stack, L. F. Allard, J. Neuefeind, D. Olds, J. Liu, and K. Page, "Synthesis and structure of synthetically pure and deuterated amorphous (basic) calcium carbonates," Chem. Commun. **53**, 2942–2945 (2017).
[11]Z. Wu, S. Lan, X. Wei, D. Olds, K. Page, B. Shen, and X.-L. Wang, "Heterogeneous nucleation in Zr-Cu-Al-Ag metallic glasses triggered by quenched-in metastable crystals—A time-resolved neutron diffraction study," Physica B (published online).
[12]J. Neuefeind, M. Feygenson, J. Carruth, R. Hoffmann, and K. K. Chipley, "The nanoscale ordered materials diffractometer NOMAD at the spallation neutron source SNS," Nucl. Instrum. Methods Phys. Res., Sect. B **287**, 68–75 (2012).

[13]D. Olds, K. Page, A. Paecklar, P. F. Peterson, J. Liu, G. Rucker, M. Ruiz-Rodriguez, M. Olsen, M. Pawel, S. H. Overbury *et al.*, "A high precision gas flow cell for performing *in situ* neutron studies of local atomic structure in catalytic materials," Rev. Sci. Instrum. **88**, 034101 (2017).

[14]D. Olds, K. V. Lawler, A. Paecklar, J. Liu, K. Page, P. F. Peterson, P. M. Forster, and J. R. Neilson, "Capturing the details of N_2 adsorption in zeolite X using stroboscopic isotope contrasted neutron total scattering," Chem. Mater. **30**, 296–302 (2018).

[15]T. Egami and S. J. Billinge, *Underneath the Bragg Peaks: Structural Analysis of Complex Materials* (Newnes, 2012), Vol. 16.

[16]J. Niedziela, R. Mills, M. Loguillo, H. Skorpenske, D. Armitage, H. Smith, J. Lin, M. Lucas, M. Stone, and D. Abernathy, "Design and operating characteristic of a vacuum furnace for time-of-flight inelastic neutron scattering measurements," Rev. Sci. Instrum. **88**, 105116 (2017).

[17]During development, previous designs of the U-tube were employed that had a maximum operating temperature of 1000 °C.

[18]P. Klosowski, M. Koennecke, J. Tischler, and R. Osborn, "NeXus: A common format for the exchange of neutron and synchroton data," Physica B **241**, 151–153 (1997).

[19]O. Arnold, J.-C. Bilheux, J. Borreguero, A. Buts, S. I. Campbell, L. Chapon, M. Doucet, N. Draper, R. F. Leal, M. Gigg *et al.*, "Mantid: Data analysis and visualization package for neutron scattering and μ SR experiments," Nucl. Instrum. Methods Phys. Res., Sect. A **764**, 156–166 (2014).

[20]R. A. Huggins, "Do you really want an unsafe battery?," J. Electrochem. Soc. **160**, A3001–A3005 (2013).

[21]Q. Wang, J. Sun, and G. Chu, "Lithium ion battery fire and explosion," Fire Saf. Sci. **8**, 375–382 (2005).

[22]S.-M. Bak, E. Hu, Y. Zhou, X. Yu, S. D. Senanayake, S.-J. Cho, K.-B. Kim, K. Y. Chung, X.-Q. Yang, and K.-W. Nam, "Structural changes and thermal stability of charged $LiNi_xMn_yCo_zO_2$ cathode materials studied by combined *in situ* time-resolved XRD and mass spectroscopy," ACS Appl. Mater. Interfaces **6**, 22594–22601 (2014).

[23]M. Kunduraci and G. Amatucci, "The effect of particle size and morphology on the rate capability of 4.7 V $LiMn_{1.5+\delta}$ $Ni_{0.5-\delta}O_4$ spinel lithium-ion battery cathodes," Electrochim. Acta **53**, 4193–4199 (2008).

[24]D. Olds, P. F. Peterson, M. K. Crawford, J. R. Neilson, H.-W. Wang, P. S. Whitfield, and K. Page, "Combinatorial appraisal of transition states for *in situ* pair distribution function analysis," J. Appl. Crystallogr. **50**, 1744–1753 (2017).

[25]S. Pacala and R. Socolow, "Stabilization wedges: Solving the climate problem for the next 50 years with current technologies," Science **305**, 968–972 (2004).

[26]M. E. Boot-Handford, J. C. Abanades, E. J. Anthony, M. J. Blunt, S. Brandani, N. Mac Dowell, J. R. Fernandez, M.-C. Ferrari, R. Gross, J. P. Hallett, R. S. Haszeldine, P. Heptonstall, A. Lyngfelt, Z. Makuch, E. Mangano, R. T. J. Porter, M. Pourkashanian, G. T. Rochelle, N. Shah, J. G. Yao, and P. S. Fennell, "Carbon capture and storage update," Energy Environ. Sci. **7**, 130–189 (2014).

[27]D. M. D'Alessandro, B. Smit, and R. L. Jeffrey, "Carbon dioxide capture: Prospects for new materials," Angew. Chem., Int. Ed. **49**, 6058–6082 (2010).

[28]S. Choi, H. D. Jeffrey, and W. J. Christopher, "Adsorbent materials for carbon dioxide capture from large anthropogenic point sources," ChemSusChem **2**, 796–854 (2009).

[29]S. K. Bhatia and D. D. Perlmutter, "Effect of the product layer on the kinetics of the CO_2-lime reaction," AIChE J. **29**, 79–86 (1983).

[30]J.-i. Ida and Y. S. Lin, "Mechanism of high-temperature CO_2 sorption on lithium zirconate," Environ. Sci. Technol. **37**, 1999–2004 (2003).

[31]J. D. Gale and A. L. Rohl, "The general utility lattice program (GULP)," Mol. Simul. **29**, 291–341 (2003).

[32]M. T. Dunstan, S. A. Maugeri, W. Liu, M. G. Tucker, O. O. Taiwo, B. Gonzalez, P. K. Allan, M. W. Gaultois, P. R. Shearing, D. A. Keen *et al.*, "*In situ* studies of materials for high temperature CO_2 capture and storage," Faraday Discuss. **192**, 217–240 (2016).